An early Lutetian carbon-cycle perturbation: Insights from the Gorrondatxe section (western Pyrenees, Bay of Biscay)

Aitor Payros,[1] Silvia Ortiz,[1] Laia Alegret,[2] Xabier Orue-Etxebarria,[1] Estibaliz Apellaniz,[1] and Eustoquio Molina[2]

[1]   A distinctive low-carbonate interval interrupts the continuous limestone-marl alternation of the deep-marine Gorrondatxe section at the early Lutetian (middle Eocene) C21r/C21n Chron transition. The interval is characterized by increased abundance of turbidites and kaolinite, a 3‰ decline in the bulk $\delta^{13}C$ record, a >1‰ decline in benthic foraminiferal $\delta^{13}C$ followed by a gradual recovery, a distinct deterioration in foraminiferal preservation, high proportions of warm-water planktic foraminifera and opportunistic benthic foraminifera, and reduced trace fossil and benthic foraminiferal diversity, thus recording a significant environmental perturbation. The onset of the perturbation correlates with the C21r-H6 event recently defined in the Atlantic and Pacific oceans, which caused a 2°C warming of the seafloor and increased carbonate dissolution. The perturbation was likely caused by the input of ^{13}C-depleted carbon into the ocean-atmosphere system, thus presenting many of the hallmarks of Paleogene hyperthermal deposits. However, from the available data it is not possible to conclusively state that the event was associated with extreme global warming. Based on our analysis, the perturbation lasted 226 kyr, from 47.44 to 47.214 Ma, and although this duration suggests that the triggering mechanism may have been similar to that of the Paleocene-Eocene Thermal Maximum (PETM), the magnitude of the carbon input and the subsequent environmental perturbation during the early Lutetian event were not as severe as in the PETM.

1.   Introduction

[2]   The early Paleogene global carbon cycle and climate evolution were closely related both in the long and short-term [*Zachos et al.*, 2001; *Kroeger and Funnell*, 2012]. A long-term decrease in $\delta^{13}C$ values during the Paleocene and early Eocene (58–51 Ma) suggests a continuous flux of isotopically light carbon into the ocean-atmosphere system, which was accompanied by a warming climate scenario. The subsequent rise in $\delta^{13}C$ values during the middle-late Eocene coincided with a cooling scenario, which eventually led to the development of permanent Antarctic ice sheets 34 Ma [*Zachos et al.*, 2001]. This long-term evolution was punctuated by several short-lived (tens to hundreds of kiloyears, kyr) episodes in which additional ^{13}C-depleted carbon was temporarily released (Table 1). Negative carbon isotope excursions (CIEs) in $\delta^{13}C$ records are among the main hallmarks of these short-lived carbon-cycle perturbations [*Zachos et al.*, 2010]. Some of these events caused extreme global warming and have therefore been referred to as hyperthermals, the Paleocene-Eocene Thermal Maximum (PETM) event being the most prominent [*Zachos et al.*, 2008]; hyperthermal conditions are also suspected for other short-lived carbon-cycle perturbations but have not been fully demonstrated to date (Table 1). These short-lived carbon-cycle perturbations had severe environmental consequences, such as increased chemical weathering and runoff on land, rises in oceanic carbonate compensation depth and transient biological changes. Pelagic sedimentary successions provide the best record of these perturbations, as their deposits stand out as clay-rich reddish layers that coincide with abrupt drops in carbonate content.

[3]   The Gorrondatxe beach section (western Pyrenees, southeastern coast of the Bay of Biscay, Lat. 43° 23′N Long. 3° 01′W; Figure 1) is one of the most complete and expanded deep-sea successions of the Ypresian/Lutetian (early/middle

[1]Department of Stratigraphy and Paleontology, Faculty of Science and Technology, University of the Basque Country (UPV/EHU), Bilbao, Spain.
[2]Department of Earth Sciences, University of Zaragoza, Zaragoza, Spain.

Corresponding author: A. Payros, Department of Stratigraphy and Paleontology, Faculty of Science and Technology, University of the Basque Country (UPV/EHU), PO Box 644, E-48080 Bilbao, Spain. (a.payros@ehu.es)

Table 1. Characteristics of Known and Suspected Paleogene Hyperthermal Events Associated to Short-Lived Carbon-Cycle Perturbations

Event	Age	CIE[a]	Warming	Duration	References
Dan-C2	65.2 Ma	−0.4–1.5‰, double peak, symmetric	4°C	100 kyr	*Quillévéré et al.* [2008]; *Coccioni et al.* [2010]
Lower C29n	65.0 Ma	−0.7‰, symmetric	Unknown	38 kyr	*Coccioni et al.* [2010]
LDE = Top C27n	61.75 Ma	−1–2‰, double peak, symmetric	2–3°C	191–200 kyr	*Bornemann et al.* [2009]; *Sprong et al.* [2011, 2012]; *Westerhold et al.* [2011]
ELPE = MPBE	59.0 Ma	−1.0‰	Unknown	50 kyr	*Petrizzo* [2005]; *Bernaola et al.* [2007]; *Dinarès-Turell et al.* [2007]
PETM = ETM1	55.8 Ma	−2.5–3‰, sharp base, gradual recovery	5–8°C	170–220 kyr	*Zachos et al.* [2005, 2008]; *Röhl et al.* [2007]; *Bowen and Zachos* [2010]
ELMO = H1 = ETM2	53.7 Ma	−0.8–1.5‰, symmetric	3–5°C	100 kyr	*Cramer et al.* [2003]; *Lourens et al.* [2005]; *Sluijs et al.* [2009]; *Galeotti et al.* [2010]; *Stap et al.* [2010]; *Leon-Rodriguez and Dickens* [2010]
H2	53.6 Ma	−0.2–0.8‰, symmetric	1–2°C	60 kyr	*Cramer et al.* [2003]; *Stap et al.* [2009, 2010]
I1	53.2 Ma	−0.1–0.7‰, symmetric	Unknown	Unknown	*Cramer et al.* [2003]; *Nicolo et al.* [2007]; *Galeotti et al.* [2010]; *Leon-Rodriguez and Dickens* [2010]
X = K = ETM3	52.5 Ma	−0.6‰, symmetric	Unknown	Unknown	*Cramer et al.* [2003]; *Agnini et al.* [2009]; *Galeotti et al.* [2010]; *Leon-Rodriguez & Dickens* [2010]
C22r-H1 to H3, C22n-H1 and H2, C21r-H1 to H5	Between 50 and 48.2 Ma	−0.7–1‰; sharp base and gradual recovery	2–4°C	40 kyr each	*Sexton et al.* [2011]
C21r-H6	47.44 Ma	−0.7–1‰, sharp base, gradual recovery	2°C at deep sea	226 kyr	*Sexton et al.* [2011]; this study
C19r	41.8 Ma	−1.1‰, symmetric	Unknown	Unknown	*Edgar et al.* [2007]
MECO (apex)	40.6–40.0 Ma	Slow +0.4‰ followed by a rapid −0.5–0.7‰ during apex; then, gradual +1‰	4°C, plus 1.5°C during the apex	500 kyr for the initial stage; 50–100 kyr for the apex	*Bohaty and Zachos* [2003]; *Bohaty et al.* [2009]; *Spofforth et al.* [2010]; *Bijl et al.* [2010]; *Edgar et al.* [2010]

[a]CIE refers to the magnitude and shape of the Carbon Isotope Excursion.

Eocene) transition [*Bernaola et al.*, 2006; *Molina et al.*, 2011]. Due to its suitability for multidisciplinary stratigraphic studies, the Global Stratotype Section and Point (GSSP) for the base of the Lutetian Stage has recently been defined in this section [*Molina et al.*, 2011]. These studies revealed the occurrence of a distinctive clay-rich interval, which is typified by sedimentological, geochemical and paleontological features that resemble those of the Paleogene short-lived carbon-cycle perturbations. The aim of this study is the analysis of the Gorrondatxe clay-rich interval in order to determine whether it represents one of the Eocene events and provide insights into its impact.

2. Geological Setting

[4] In Eocene times the Gorrondatxe area was located between mainland Europe and the Iberian craton (Figure 1), in a narrow marine gulf, approximately 1500 m deep, that opened into the Atlantic Ocean at 35°N paleolatitude [*Payros et al.*, 2006]. A 2300 m thick sedimentary succession

accumulated during early-middle Eocene times, the section studied herein extending from 900 to 1100 m.

[5] *Payros et al.* [2006, 2007] defined three turbidite-poor intervals and three turbidite-rich intervals, the former being typified by warm-water planktic foraminiferal assemblages and the latter by cool-water associations (Figure 1). This correlation points toward climatic variations as a possible driving mechanism for both sedimentary and biotic changes, and allows interpretation of the succession in terms of depositional sequences. *Payros et al.* [2009b] further showed that these depositional sequences can be correlated worldwide and coincide with oceanic temperature variations recorded by oxygen isotopes in several deep-sea sites. This suggests that the depositional sequences may be the result of climatically driven eustatic sea level changes [*Payros et al.*, 2009b].

[6] The 200 m thick succession studied herein is included within the upper part of the second turbidite-poor interval and corresponds to the upper part of the transgressive systems tract and the highstand systems tract of a depositional sequence that extends from the latest Ypresian to the earliest Lutetian
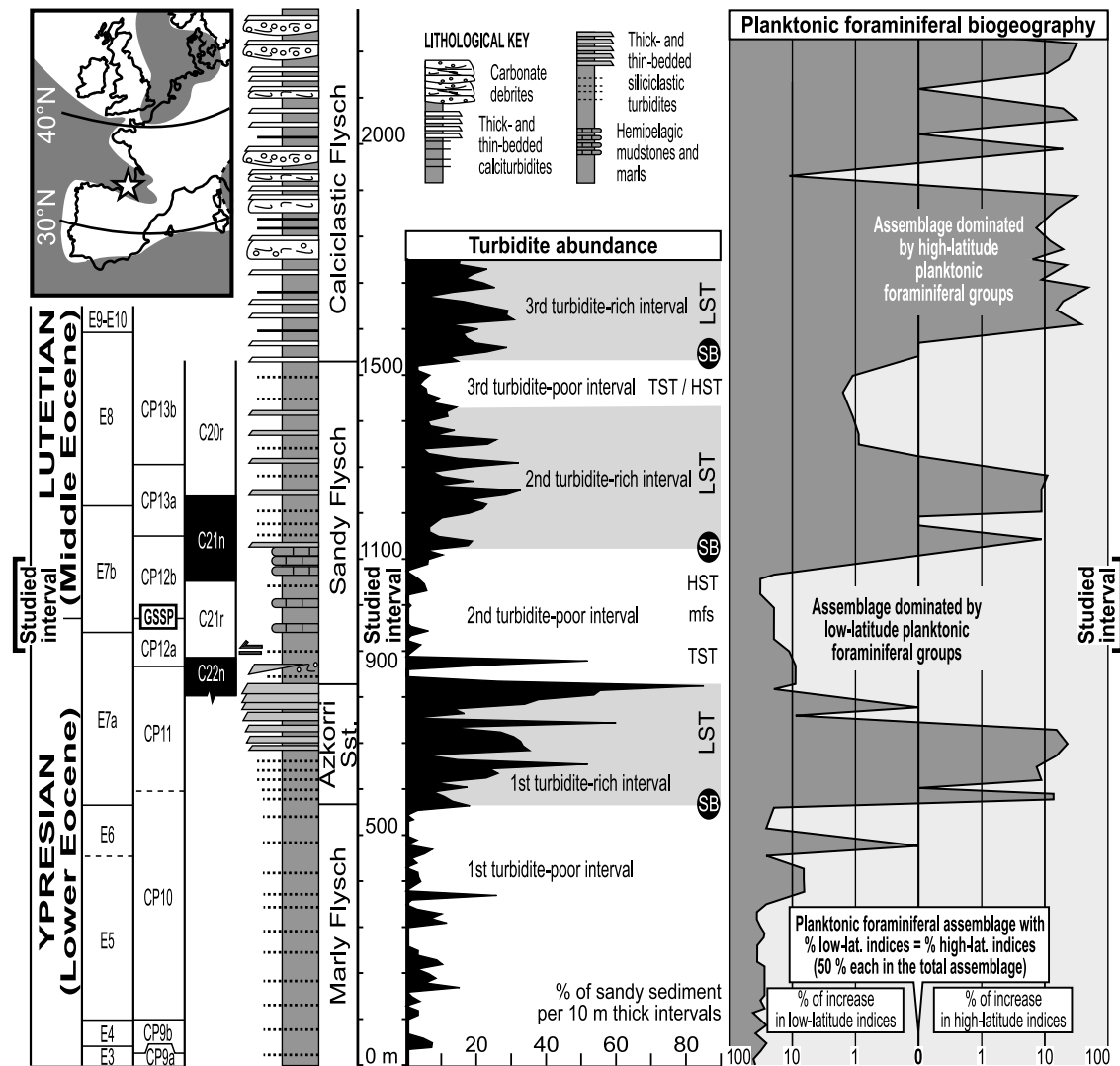
Figure 1. Inset: paleogeographic location (white star) of the Gorrondatxe area (white: land; gray: sea). Simplified litholog of the Eocene deep-marine succession in the Gorrondatxe area, showing chronostratigraphy (planktic foraminiferal E scale of *Wade et al.* [2011]; calcareous nannofossil CP scale of *Okada and Bukry* [1980]), distribution of turbidites, depositional sequences (SB: sequence boundary; LST: lowstand systems tract; TST: transgressive systems tract; mfs: maximum flooding surface; HST: highstand systems tract), and planktic foraminiferal paleobiogeographic indices; based on *Payros et al.* [2006]. The succession studied herein extends from 900 to 1100 m.

(Figure 1). This succession is composed of alternating hemipelagic limestones and marls interspersed with thin-bedded turbidites [*Payros et al.*, 2006]. These characteristics allowed identification of precession-related limestone-marl couplets of 21 kyr and eccentricity-related bundles of 100 kyr (Figure 2) [*Payros et al.*, 2009a, 2011]. Using the cyclostratigraphic approach, *Payros et al.* [2011] calculated that the sedimentation rate was 12.8 cm/kyr.

3. Material and Methods

[7] A detailed, bed-by-bed litholog was produced by measuring the 200 m thick section. In order to define sedimentologically distinct intervals, the type and proportion of turbiditic and hemipelagic facies were accurately determined following the procedure used by *Payros et al.* [2007]

(information on analytical methods and quantitative results is available in the auxiliary material; see Figures S1 and S2 and Tables S1–S9).[1]

[8] Fifty-two unweathered samples of hemipelagic mudstones were collected in order to analyze their mineralogical content by X-ray diffraction (XRD) using a Philips PW1710 diffractometer at the University of the Basque Country. Semiquantitative abundance estimates were obtained using the intensity (area) of the major XRD reflections with correcting factors.

[9] Thirty-nine samples were collected for the analysis of benthic foraminifera, increasing the sampling resolution of *Ortiz et al.* [2011] within the studied interval. The

---

Figure 2. LSPAN Litholog of the succession studied at Gorrondatxe, showing chronostratigraphy, precession-driven mudstone-marl couplets, variations in the percentage of turbiditic and hemipelagic sediments (Table S1), and carbonate content of the latter (Table S4). A, B, C and D correspond to stratigraphic intervals discussed in the text. The 0 m level corresponds to the 900 m level of the general Eocene succession shown in Figure 1.
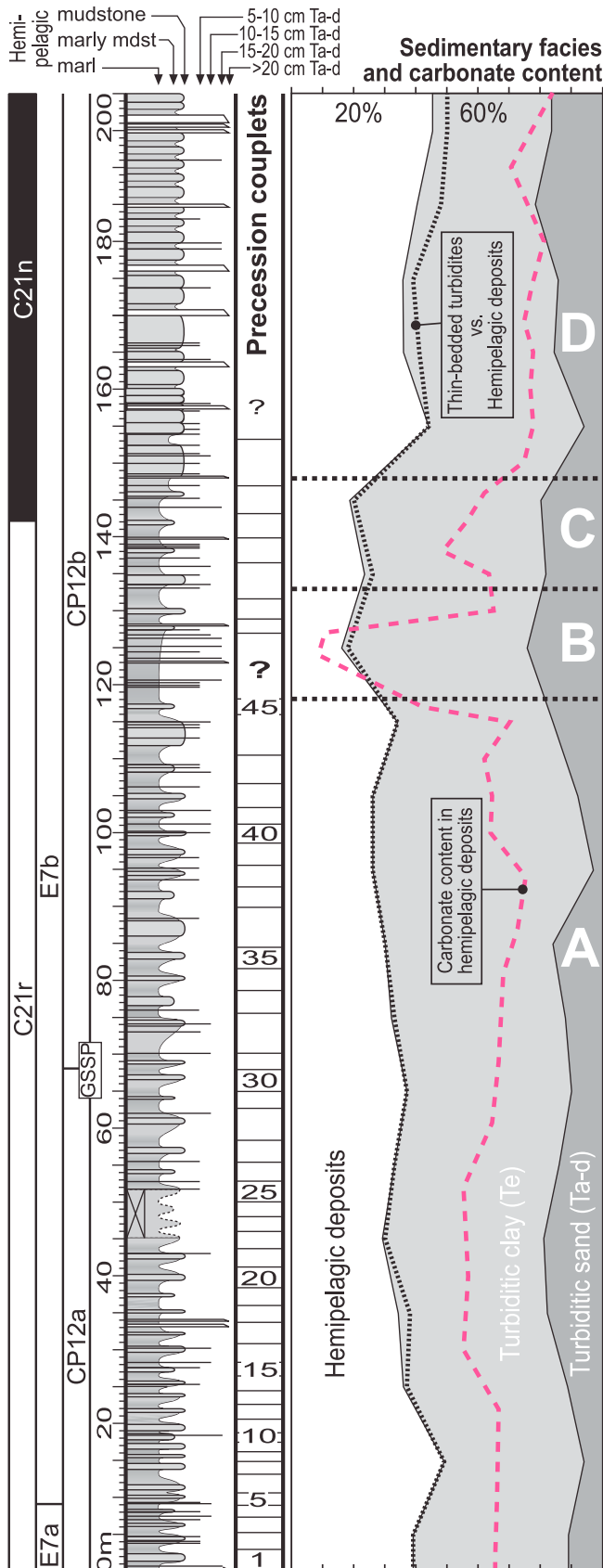
quantitative analysis of benthic foraminifera was based on representative splits of approximately 300 specimens obtained using a modified Otto micro-splitter. In order to determine the environmental evolution, shallow-water allochthonous taxa, which were probably transported downslope by turbidity currents, were removed from the foraminiferal counts [*Ortiz et al.*, 2011]. Therefore, benthic foraminiferal percentages refer to the autochthonous assemblages, unless otherwise indicated.

[10] Thirty-two samples were analyzed for their calcium carbonate content. The percentage of carbonate was determined volumetrically in a gauge calcimeter at the University of Zaragoza following standard methods.

[11] Thirty bulk (whole rock) samples were analyzed for carbon and oxygen stable isotope ratios. Samples were systematically collected from fresh hemipelagic mudstones, which are thought to yield the most reliable results [*Schmitz et al.*, 1997, 2001]. In order to test the validity of this assumption, forty additional samples were prepared for stable isotope analysis by extracting *Nuttallides truempyi* specimens from key levels. The isotopic analysis was performed at the Bloomsbury Environmental Isotope Facility (BEIF) of University College London. Precision of all internal (BDH, IAEA and IFC) and external standards (NBS19) is ± 0.03 for $\delta^{13}C$ and ± 0.08 for $\delta^{18}O$. All values are reported in the Vienna Pee Dee Bee notation (VPDB) relative to NBS19.

[12] Planktic foraminifera were not specifically analyzed in this study, but previously published information was compiled from *Payros et al.* [2006]. The latter study aimed at the paleobiogeographical evolution of the entire 2300 m thick Eocene succession, ranking planktic foraminiferal species as low, middle, and high latitude taxa. Ichnofossil information was compiled from *Rodríguez-Tovar et al.* [2010].

4. Results

4.1. Sedimentary and Geochemical Trends

[13] Four distinct stratigraphic intervals (A-D) were defined in the studied succession using sedimentological criteria, combined with mineralogical and geochemical data (Figure 2).

[14] Interval A, up to 118 m, is characterized by the regular alternation of hemipelagic mudstones and marls (Figures 2 and S1), which represent 21 kyr precession couplets [*Payros et al.*, 2009a, 2011]. Intercalated turbidites are commonly a few millimeters thick. The proportion of hemipelagic deposits ranges from 26 to 49%, averaging out at 34% (Figure 2 and Table S1). Depending on the hemipelagic lithology, the carbonate content varies between 42 and 75%, the average being 64% (Figure 2 and Table S4). XRD results show that calcite content varies between 25 and

Figure 3. X-ray diffraction mineralogy of the Gorrondatxe hemipelagic sediments (Tables S2 and S3); ch refers to chlorite. The kaolinite/smectite ratio is plotted on a two-sided, symmetric semilogarithmic graph as the percentage of deviation from a neutral content of 50% in each mineral.

85%, averaging out at 59% (Figure 3 and Table S2). Clay minerals make up 10–57% of the total mineralogy (average 28%; Tables S2 and S3), mainly consisting of smectite (33–69%; average 44%) and illite (26–49%; average 40%) and containing variable amounts of kaolinite (0–24%; average 10%) and chlorite (0–16%; average 6%). The kaolinite/smectite ratio is variable but consistently below 1 (range: 0–0.73; average: 0.23). Bulk $\delta^{13}C$ values are positive, ranging from 0.06 to 0.66‰, and average out at 0.43‰ (Figure 4 and Table S5). The *Nuttallides truempyi* $\delta^{13}C$ trend parallels that of the bulk samples, albeit with somewhat lower absolute values (between −0.16 and 0.45‰, average 0.23‰; Figure 4 and Table S6).

[15] Interval B (118–133 m) records an increase in the abundance and thickness of sandy turbidites and a concomitant decrease in the percentage of hemipelagic deposits (16–

23%; average 19%). Gray and fewer reddish marl layers dominate the hemipelagic deposits (Figure S1). The conspicuous near absence of hemipelagic limestone beds hampers identification of the astronomical signal in the lower part of Interval B (Figure 2). The scarcity of limestones is also expressed by an abrupt drop in carbonate content to an average value of 28.2% (minimum of 8.7%). In XRD analysis the average calcite content decreases to 29%, whereas clay minerals increase to 46% (Figure 3). Clay minerals show an increase in kaolinite (20–30%; average 25%) and a decrease in smectite (9–35%; average 26%), resulting in a higher kaolinite/smectite ratio (range: 0.57–3.33; average: 0.96). The $\delta^{13}C$ records show a shift to negative values in the lower part of Interval B, reaching minimal values at 124 m. The CIE is of −3.12‰ or −2.99‰ in the bulk record, depending on whether the average $\delta^{13}C$ value of Interval A
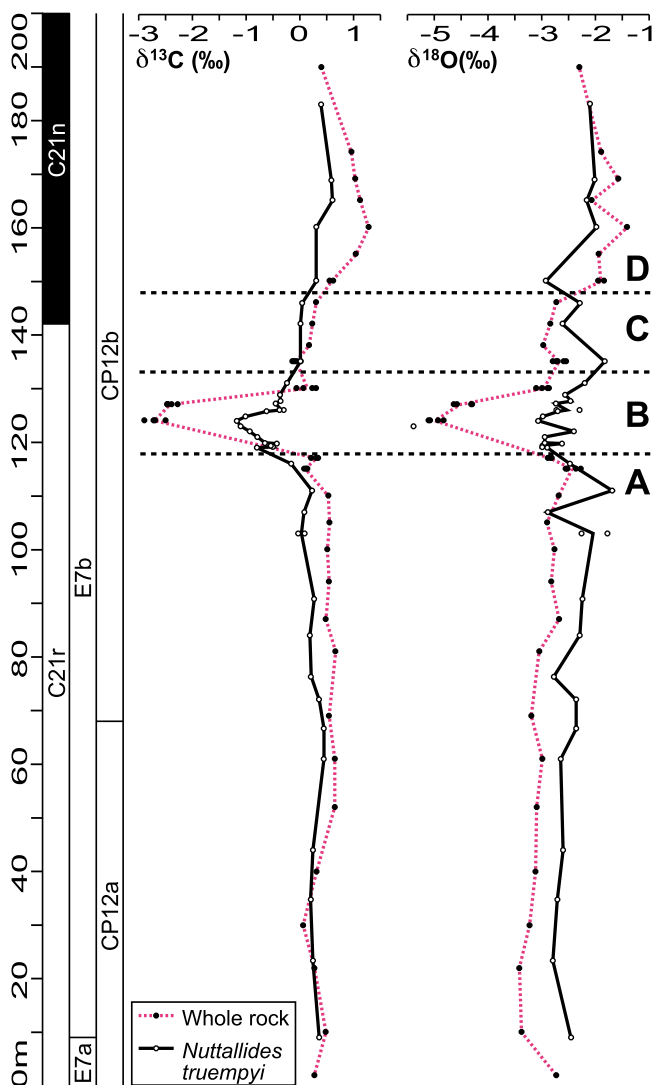
Figure 4. Stable isotope results from the Gorrondatxe hemipelagic mudstones (Table S5) and from *Nuttallides truempyi* (Table S6).

or only that of its uppermost sample is considered. On the same basis, the *Nuttallides truempyi* CIE is of −1.4‰ or −1.01‰. Carbon stable isotope ratios recover in the upper part of Interval B, though still with predominantly negative values (Figure 4).

[16] Interval C (133–148 m) shows a progressive return to the characteristics observed in Interval A. The abundance of thick-bedded turbidites decreases, although the average proportion of hemipelagic deposits remains low (19%) due to the abundance of thin-bedded turbidites (Figure 2). Conversely, the carbonate content progressively increases to 62.1%, averaging out at 52% (70% in XRD; Figure 3). This allows a tentative definition of precession-driven mudstone-marl couplets. Clay minerals also record a progressive return toward Interval A characteristics (average content: 21%; kaolinite/smectite ratio: 0.51). The $\delta^{13}C$ record shows a return to positive values and a gradual upward increase, from

−0.07 to 0.30‰ in the bulk record and from 0.01 to 0.04‰ in the *Nuttallides truempyi* record (Figure 4).

[17] Interval D, from 148 m upward, is characterized by a noticeable increase in the abundance of hemipelagic mudstones (Figures 2 and S1). Although a few thick-bedded turbidites occur, the abundance of thin-bedded turbidites decreases, resulting in the lowest turbiditic percentage of the section and the highest proportion of hemipelagic deposits (36–45%, average 40%). These changes are expressed by an increase in carbonate content (average 77.3% in calcimeter analysis and 84% in XRD analysis; Figures 2 and 3). The clay mineral content (average 11%) and composition (near absolute dominance of smectite and illite; average kaolinite/smectite ratio 0.02) resemble those found in Interval A. In the lower part of Interval D, $\delta^{13}C$ values exceed those of all of the underlying intervals, ranging from 0.40 to 1.28‰ in the bulk record and from 0.30 to 0.60‰ in the *Nuttallides truempyi* record (Figure 4). However, a gradually decreasing trend prevails in the upper part of Interval D, reaching values that are again similar to those in Interval A.

4.2. Biotic Trends

[18] The following foraminiferal and trace fossil assemblages were observed in the aforementioned intervals.

[19] Interval A: Low-latitude and warm-water planktic foraminiferal taxa dominate (60% of the assemblages; Figure 1 and Table S8). Foraminiferal test preservation is moderately good. Allochthonous benthic foraminiferal taxa are generally scarce (average 6.5%; Figure 5 and Table S7). The percentage of planktic foraminifera averages out at 94%, which is common in bathyal settings. The autochthonous benthic foraminiferal assemblage is highly diverse and characterized by calcareous taxa (mainly bolivinids, uniserial calcareous, *Cibicidoides* species, buliminids and *Nuttallides truempyi*), which make up to 79% of the assemblages (Figure 5 and Table S7). Agglutinated foraminifera are strongly dominated by organic-cemented taxa (88.5% of agglutinated assemblages), mainly trochamminids (e.g., *Ammosphaeroidina pseudopauciloculata*; see auxiliary material) and astrorhizids (e.g., *Bathysiphon*, *Nothia* and *Rhabdammina* species). *Rodríguez-Tovar et al.* [2010] documented abundant and diverse trace fossils throughout Interval A, including both pre-depositional graphoglyptids and post-depositional ichnotaxa (Table S9), which indicate a dominant agrichnial behavior, whereas others like paschich-nia, fodinichnia and chemichnia were rare.

[20] Interval B: Major biotic changes occur in Interval B. The proportion of low-latitude, warm-water planktic foraminiferal taxa increases to 70% (Figure 1 and Table S8). Preservation is poorer than in Interval A, foraminifers showing corroded tests and broken chambers (Figure S2). Additionally, a decrease in the percentage of planktic foraminifera occurs (minimum of 86%) in the middle part of Interval B, followed by a recovery in its upper part (Figure 5 and Table S7). The diversity of autochthonous benthic foraminiferal taxa decreases in Interval B, most distinctively in its middle part. Epifaunal morphogroups (up to 63%) and agglutinated taxa (up to 72%; mostly organic-cemented trochamminids, *Spiroplectammina spectabilis* and *Pseudoboli-vina* sp. A) dominate the assemblages in the middle part of Interval B, where a significant increase in *Globobulimina*
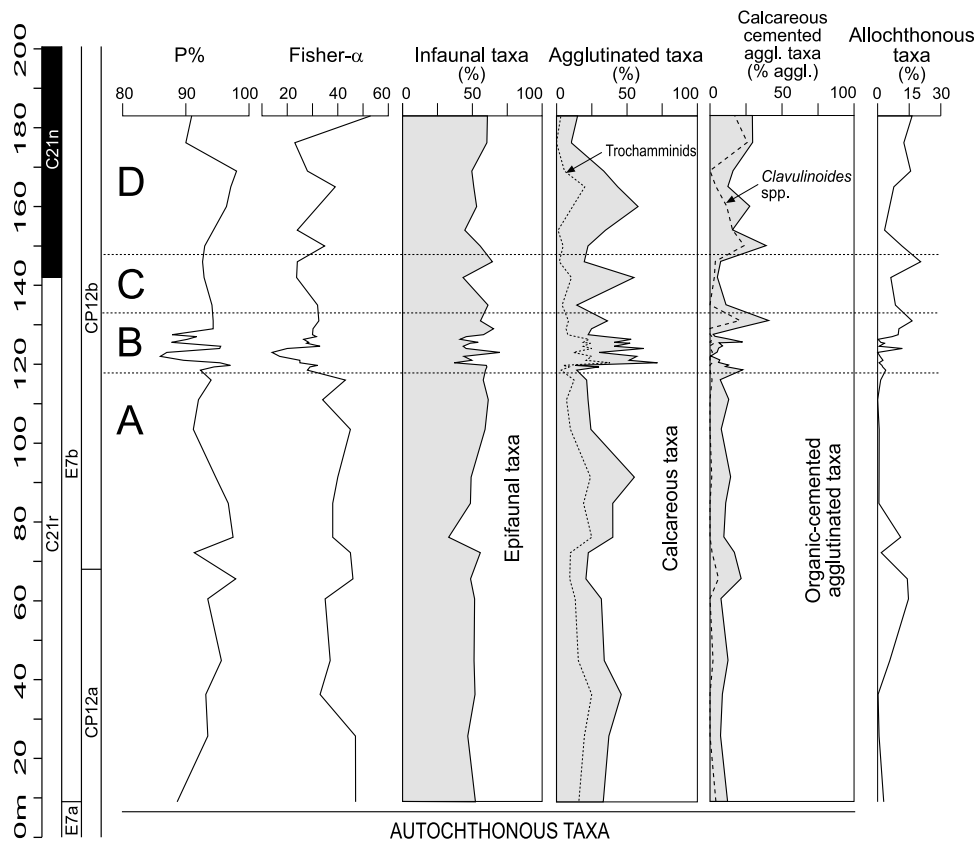
Figure 5. Foraminiferal indices at Gorrondatxe (Table S7): percentage of planktic foraminifera (P%), autochthonous benthic foraminiferal Fisher-α diversity index, percentages of infaunal, agglutinated and calcareous-cemented agglutinated (calcareous- to calcareous- plus organic-cemented agglutinated taxa ratio) autochthonous benthic taxa, and percentages of allochthonous benthic taxa.

species, usually with pyrite fillings, occurs (Figures 6 and S2 and Table S7). Trace fossils show a prominent decrease in diversity and abundance, with a near-disappearance of graphoglyptids (Table S9) [*Rodríguez-Tovar et al.*, 2010].

[21] Interval C: The proportion of low-latitude, warm-water planktic foraminifera remains high (Figure 1 and Table S8). Allochthonous benthic foraminiferal taxa are common (17%) and diversity of the autochthonous assemblage is moderately low (Figure 5 and Table S7). *Aragonia aragonensis* and coarse-grained astrorhizids show abundance peaks (4.4 and 34.4%, respectively), and *Globobulimina* species are common (Figure 6 and Table S7). Apart from these features, foraminiferal assemblages are similar to those from Interval A (Table S7). Trace fossil assemblages remain similar to those of Interval B (Table S9) [*Rodríguez-Tovar et al.*, 2010].

[22] Interval D: Most of the biotic characteristics in Interval D are similar to those in Interval A. The proportion of low-latitude, warm water planktic foraminiferal taxa remains high in the lowermost part of Interval D but returns to Interval A values in its upper part (Figure 1 and Table S8). The percentage of planktic foraminifera (93.5%) and high benthic foraminiferal diversity with dominance of calcareous taxa resemble the characteristics of Interval A. However, allochthonous taxa are common (16%) in Interval D (Figure 5). The

percentage of calcareous-cemented agglutinated foraminifera (mainly *Clavulinoides* species; Figure 5) significantly increases in Interval D and the abundance of *Aragonia aragonensis* (up to 6.5%) and radiolarians increase in its middle-upper part (Figure 6). Low abundance and diversity of trace fossils prevail in Interval D (Table S9); most ichnotaxa are post-depositional, winding and meandering structures, showing dominant pascichnial behavior [*Rodríguez-Tovar et al.*, 2010].

5. Environmental Evolution

[23] The high diversity of calcareous benthic foraminiferal assemblages in Interval A, the abundance of agglutinated taxa and the varied trace maker behaviors inferred from trace fossils are typical of deep-sea clastic substrates and indicate a stable, low-energy, well-oxygenated and oligotrophic to mesotrophic environment [*Rodríguez-Tovar et al.*, 2010; *Ortiz et al.*, 2011].

[24] The sedimentological, geochemical and biotic characteristics of Interval B record a transient change of the stable environmental conditions that had long prevailed in Interval A. The environmental perturbation is biotically recorded by benthic foraminiferal assemblages that decrease in diversity and are enriched in opportunistic agglutinated taxa (trochamminids and *Spiroplectammina* species; Figure 6) [*Kauffman et al.*, 1996]. These changes, together with a decrease in the
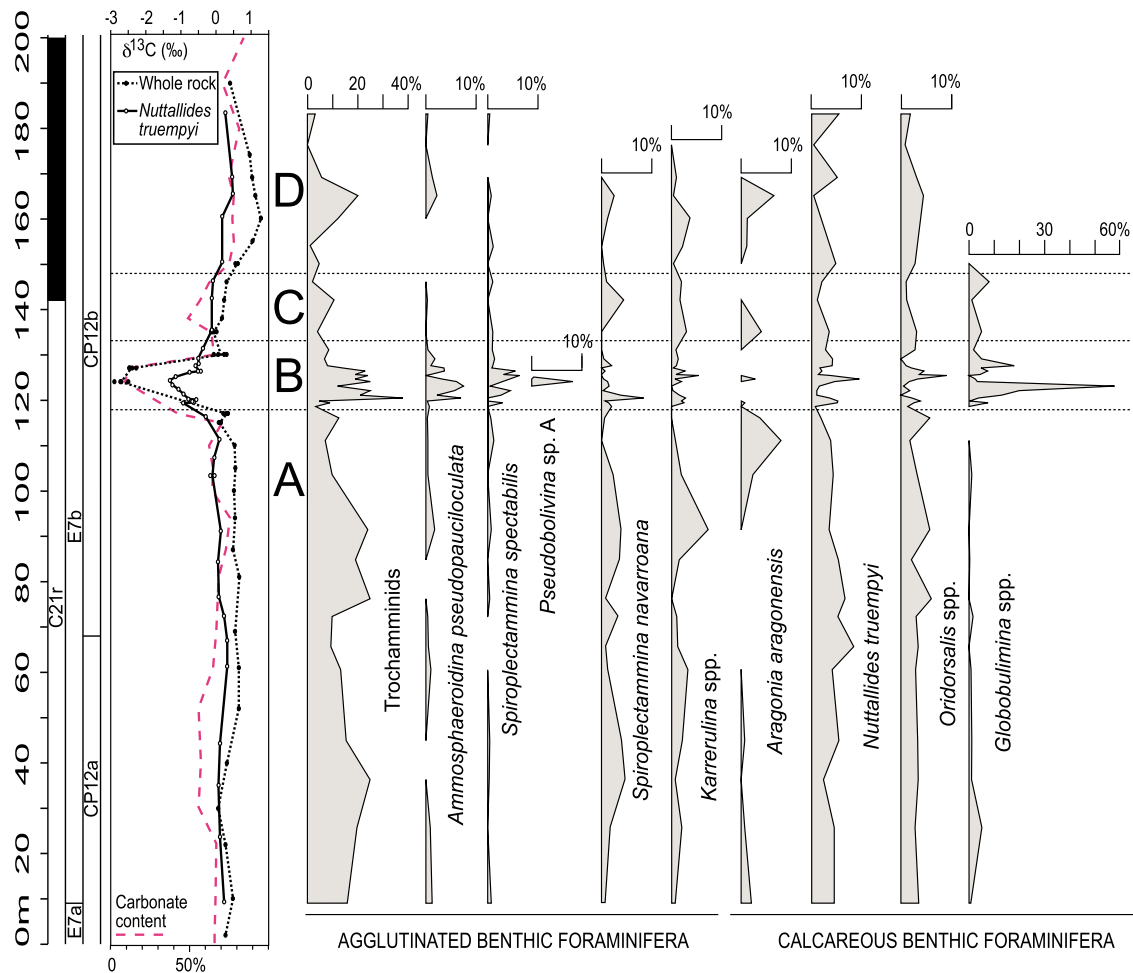
Figure 6. Stratigraphic distribution and relative abundance of selected autochthonous benthic foraminiferal taxa (Table S7) plotted against the carbonate content and stable isotope curves at Gorrondatxe. Note the different scales for trochamminids and *Globobulimina*.

abundance and diversity of trace fossils, coincide with a deterioration in the preservation of foraminifera, a reduced percentage of planktic foraminifera and an increase in the proportion of warm-water planktic foraminiferal taxa. *Nguyen et al.* [2011] showed that the enrichment in warm-water *Acarinina* and *Morozovella* may result from dissolution, as these taxa are more resistant than *Subbotina* and *Igorina*. Although dissolution affected some of the Interval B carbonate components, several lines of evidence suggest that this process alone cannot account for the increase in warm-water planktic foraminiferal species (Table S8): first, *Acarinina* and *Morozovella* are not the only warm-water taxa identified in Gorrondatxe; second, dissolution-prone *Subbotina* and *Igorina* species occur throughout the section, including Interval B; finally, the high proportion of warm-water taxa can be found up to the lower part of Interval D, where there is no evidence of dissolution and carbonate content is at its highest. The fossil record thus shows that the environmental perturbation of Interval B affected both seafloor and pelagic ecosystems.

[25] The physical expression of the environmental perturbation corresponds to an increase in siliciclastic sand and clay input, leading to diminished carbonate hemipelagic sedimentation (Figures 2 and 3). The increase in kaolinite and decrease

in smectite must have occurred at formation, since early diagenetic authigenesis of smectite at the water-sediment interface only occurs under very low sedimentation rates [*Thiry*, 2000], which is not the case in Gorrondatxe. It could be argued that the mineralogical change simply reflects increased turbiditic currents in Interval B, as kaolinite particles are generally larger than smectite particles and this leads to higher kaolinite proportion in high-energy environments [*Thiry*, 2000; *Gertsch et al.*, 2010]. However, other turbidite-rich stratigraphic slices of the Gorrondatxe section do not show comparable increases in kaolinite (Figure 3). Neither illite nor chlorite, which are hydrodynamically similar to kaolinite, show comparable increases in Interval B, discounting the possibility that the kaolinite spike was solely caused by hydrodynamic segregation of clay particles. Therefore, this event reflects a change in the abundance and type of clay minerals inherited from continental source areas.

[26] Stable isotopes also show notable changes in Interval B (Figure 4), but their interpretation is not straightforward. As oxygen isotope values are prone to diagenetic alteration during burial [*Marshall*, 1992], they were not used for paleotemperature estimations but only to assess the degree of diagenetic overprinting on the $\delta^{13}C$ record [*Schmitz et al.*, 2001]. The bulk $\delta^{13}C$ record of Interval B shows a

significant decline accompanied by very low $\delta^{18}O$ values (−5 to −4‰). This may reflect significant diagenetic alteration that could have affected bulk $\delta^{13}C$ values. This hindrance was overcome through comparison with the *Nuttallides truempyi* record, as the *Nuttallides truempyi* $\delta^{18}O$ values are not particularly low and are relatively stable (between −3.08 and −1.69‰) throughout the section. Moreover, these values co-vary neither with $\delta^{13}C$, nor with lithology (Figure 4), suggesting that the diagenetic overprinting on the *Nuttallides truempyi* $\delta^{13}C$ is negligible. Consequently, the decline and recovery of *Nuttallides truempyi* $\delta^{13}C$ across Interval B must be regarded as primary signals. The magnitude of the *Nuttallides truempyi* negative CIE is greater than 1‰, but to err on the side of caution this conservative value will be used hereafter for further evaluations. Although the CIE in Interval B is regarded as synsedimentary, it could be considered to be within the range of natural variability, as turbiditic settings such as Gorrondatxe receive different sedimentary components, including periplatform aragonite, which might affect the $\delta^{13}C$ record. However, *Reuning et al.* [2002, 2005] showed that a higher neritic aragonite supply produces higher $\delta^{13}C$ values. The occurrence of the lowest $\delta^{13}C$ values in Interval B, precisely coinciding with the highest turbidite content, suggests that the $\delta^{13}C$ record is not affected by changes in the proportion of sedimentary components. Moreover, the stable $\delta^{13}C$ values in Interval A (Figure 4) confirm that the $\delta^{13}C$ decline in Interval B is not an artifact, but rather part of the environmental change. Similarly, the coherent progressive recovery of $\delta^{13}C$ through intervals B-C-D in the *Nuttallides truempyi* record, which is defined regardless of lithology, shows that this trend is also linked to the paleoenvironmental evolution.

[27] The characteristics observed in intervals B-C-D bear many of the hallmarks of deep-sea clay-rich horizons accumulated during the Paleogene short-lived carbon-cycle perturbations (Table 1). From this, the following environmental evolution can be envisaged for the Gorrondatxe section.

5.1. Warming and Dissolution Due to ^{13}C-Depleted Carbon Input

[28] Warming of the sea surface is inferred from the increase in low-latitude planktic foraminifera in Interval B (Figure 1). A low carbonate content, a decrease in the percentage of planktic foraminifera and a distinct deterioration in foraminiferal preservation in the middle part of Interval B are indicative of deep-sea carbonate dissolution [*Leon-Rodriguez and Dickens*, 2010] and suggest corrosive bottom waters, probably related to a rise in the lysocline. Shoaling of the lysocline and seabed carbonate dissolution are associated with most Paleogene carbon-cycle perturbation events [*Zachos et al.*, 2005].

[29] Sea-surface warming and deep-sea carbonate dissolution point to increased pCO2 [*Zachos et al.*, 2010]. A coeval $\delta^{13}C$ decline (Figure 4) suggests that this might have been caused by a massive injection of isotopically light carbon into the ocean-atmosphere system, as in other Paleogene short-lived environmental perturbations. The sources and input mechanisms of the ^{13}C-depleted carbon added in each of the Paleogene events were probably variable, but methane released from deep-sea thermogenic degassing and/or clathrate dissociation are most commonly invoked [*Dickens et al.*,

1995, 1997; *Zachos et al.*, 2001, 2005, 2008; *Svensen et al.*, 2004; *Dickens*, 2011]. The relatively long recovery of the Gorrondatxe event (see below) suggests that the added carbon was derived from buried reservoirs [*Norris and Röhl*, 1999; *Quillévéré et al.*, 2008]. The benthic foraminiferal −1‰ CIE at Gorrondatxe can be explained by a release of at least 650 Gt of carbon from clathrates ($\delta^{13}C$: −60‰), a release of 1700 Gt of carbon from sedimentary organic matter ($\delta^{13}C$: −22‰), or a combination of both [*Sexton et al.*, 2011].

[30] The increase in turbiditic sediments in Interval B (Figures 2 and 3) suggests that mechanical weathering increased in terrestrial source areas and thus resembles many Paleogene carbon-cycle perturbation events [*Bolle and Adatte*, 2001; *Schmitz et al.*, 2001; *Schmitz and Pujalte*, 2003, 2007; *Nicolo et al.*, 2007; *Agnini et al.*, 2009; *Sluijs et al.*, 2009, 2011; *Spofforth et al.*, 2010]. Clay minerals from Gorrondatxe support this assumption. The kaolinite spike at Interval B could be a result of increased erosion of pre-existing kaolinite-rich sediments in terrestrial environments. Alternatively, it could be a consequence of changing from a warm, semiarid climate with seasonally fluctuating humidity levels to warm, perennial humid conditions: the former would have produced smectite-dominated vertisol soils, whereas the latter would have been conducive to kaolinite-rich soils; in fact, high atmospheric CO_2 levels significantly accelerate the formation of kaolinitic clays [*Thiry*, 2000]. Whatever the case, the kaolinite spike implies increased weathering rates and runoff on the adjacent continent, which in all likelihood were a consequence of increased rainfall and, arguably, higher temperature and atmospheric pCO2. A kaolinite spike also characterizes many PETM successions [*Robert and Kennett*, 1992, 1994].

5.2. Ecological Impact

[31] The environmental perturbation during Interval B affected not only surface waters [*Payros et al.*, 2006], but also the deep-sea ecosystem. The high proportion of deep-water organic-cemented agglutinated foraminifera in Interval B could be related to either carbonate corrosivity or high supply of clastic material. However, additional changes must have affected the seabed, as there is an increase in opportunistic taxa that take advantage of high-stress, strongly fluctuating environments [*Kauffman et al.*, 1996]. Similar peaks of opportunistic taxa have been documented in some hyperthermal events [*Thomas*, 2003, 2007; *Alegret et al.*, 2005, 2009a, 2009b, 2010; *Agnini et al.*, 2009; *Giusberti et al.*, 2009; *Alegret and Ortiz*, 2010; *Coccioni et al.*, 2010]. The extinction of deep-sea calcifiers during the PETM and other hyperthermal events has not only been attributed to carbonate undersaturation, but also to changes in oxygenation, food supply and bottom water temperatures [*Alegret et al.*, 2005, 2009a, 2009b, 2010; *Thomas*, 2007; *Ridgwell and Schmidt*, 2010; *Stap et al.*, 2010; *Winguth et al.*, 2012].

[32] During most Paleogene events the increased sediment supply was coupled with an increase in terrestrially derived nutrients, which in some cases led to enhanced productivity followed by bottom water dysoxia [*Colosimo et al.*, 2006; *Zachos et al.*, 2008; *Bowen and Zachos*, 2010; *Chun et al.*, 2010; *Luciani et al.*, 2010; *Spofforth et al.*, 2010]. The Gorrondatxe benthic foraminifera and trace fossils point to increased runoff in Interval B, but do not support an increase in productivity, as oligotrophic to mesotrophic conditions

prevailed. However, the peak in pyrite-filled *Globobulimina* species (Figures 6 and S2), which are deep-infaunal taxa, points to low-oxygen conditions or abundant refractory organic matter at the seabed during Interval B [*Freudenthal et al.*, 2001; *Fontanier et al.*, 2005]. Although trace fossils confirm an increase in deeply buried plant detritus and lower oxygenation in the sediment [*Rodríguez-Tovar et al.*, 2010], which may have resulted from CH_4 oxidation in the deep ocean [*Colosimo et al.*, 2006], the high proportion of epifaunal benthic foraminifera, the occurrence of trace fossils and the absence of laminated sediments suggest that the seafloor remained oxygenated.

5.3. Recovery and Aftermath

[33] A progressive recovery of environmental conditions is observed in Interval C. Thick-bedded turbidites decrease and clay mineral suites become similar to those found in Interval A (Figures 2 and 3), indicating an overall reduction in continental rainfall and runoff. However, not all proxies show a coeval recovery in Interval C. The recovery of carbonate content to pre-event levels occurred slightly faster than the recovery of $\delta^{13}C$ values (Figure 4). A similar decoupled evolution has also been observed in, and partly modeled for, the PETM, ETM2 and MECO events [*Dickens et al.*, 1997; *Zachos et al.*, 2005; *Bohaty et al.*, 2009; *Stap et al.*, 2009]. The restoration of oceanic ecological conditions took even longer. Planktic foraminifera show that warm conditions persisted during Interval C and the beginning of Interval D (Table S8). Benthic foraminiferal diversity does not reach Interval A values, and opportunistic species (*A. aragonensis*, *Spiroplectammina navarroana*) are still present (Figures 5 and 6); these species were also common during the recovery of the PETM and other hyperthermal events [*Alegret et al.*, 2009a, 2009b; *Giusberti et al.*, 2009]. Trace fossil assemblages did not recover in the rest of the Gorrondatxe succession, but this may simply reflect a change in substrate composition rather than prevalence of adverse sea-bottom environmental conditions [*Rodríguez-Tovar et al.*, 2010].

[34] The lower part of Interval D records a transient overcompensation phase in which the pre-perturbation carbonate content and $\delta^{13}C$ values were temporarily exceeded (Figures 2 and 4), resembling the aftermath of many short-lived carbon-cycle perturbations [*Dickens et al.*, 1997; *Zachos et al.*, 2005, 2008; *Bohaty et al.*, 2009; *Stap et al.*, 2009, 2010; *Leon-Rodriguez and Dickens*, 2010; *Spofforth et al.*, 2010]. These features, together with the higher proportion of calcareous-cemented agglutinated foraminifera (Figure 5), show that, owing to seawater HCO_3^- oversaturation and enhanced alkalinity, the lysocline was deeper at this time than prior to the perturbation. The long recovery and aftermath of the Gorrondatxe event (see below) suggest that these conditions were driven by increased continental silicate weathering under high atmospheric CO_2 concentrations [*Ridgwell and Edwards*, 2007; *Zeebe*, 2012]. The weathered terrestrial HCO_3^- had a more positive $\delta^{13}C$ signal, driving the positive shift in the $\delta^{13}C$ values [*Spofforth et al.*, 2010]. The transient peak of radiolarians at the beginning of Interval D was also favored by increased silicate weathering, which produced better preservation conditions for siliceous plankton.

[35] Consumption of atmospheric CO_2 through silicate weathering processes eventually diminished the carbon-gas-driven greenhouse effect and prompted a concomitant climatic cooling. These changes are respectively recorded by the progressive return of the $\delta^{13}C$ signal to pre-event average values (Figure 4) and by an increase in the abundance of cool-water planktic foraminifera in the upper part of Interval D (Figure 1 and Table S8).

5.4. Timing

[36] The onset of Interval B occurs 15 precession-driven mudstone-marl couplets above the Lutetian GSSP (Figure 2), which was dated at 47.76 Ma [*Payros et al.*, 2011; *Molina et al.*, 2011] using the *Gradstein et al.* [2004] time scale. Accepting an approximate duration of 21 kyr for each couplet, the onset of Interval B is dated at 47.44 Ma. The recovery phase through Interval C includes the C21r/C21n chron reversal at 142 m, which was dated at 47.235 Ma by *Gradstein et al.* [2004], and extends for another precession-driven couplet. These data yield a total length of 226 kyr for the Gorrondatxe environmental perturbation.

6. A Global Event

[37] The environmental reconstruction at Gorrondatxe raises the question of whether the perturbation was a regional or global phenomenon. The Ypresian/Lutetian sedimentary record from the tropical western Atlantic Ocean (ODP 1258, at 3000 m paleodepth; *Sexton et al.* [2011]) provides compelling evidence for rendering the perturbation as global. *Sexton et al.* [2011] described 13 Ypresian/Lutetian events characterized by 0.7–1‰ negative CIEs, lower than average $\delta^{18}O$ values (i.e., warming events), and increased carbonate dissolution. Six of the events occur in Chron C21r (Figure 7). The oldest five events (C21r-H1 to H5) have no clear equivalent at Gorrondatxe but the youngest event (C21r-H6), which is characterized by a 0.7‰ decrease in $\delta^{13}C$, matches precisely the onset of Interval B. The correlation is supported by biostratigraphic data, as the C21r-H6 event is preceded by the last appearance datum of the calcareous nannofossil *Discoaster lodoensis*; in Gorrondatxe the highest occurrence of this taxon was found in the uppermost beds of Interval A, at 115 m [*Bernaola et al.*, 2006]. The C21r-H6 event shows a 0.4‰ decrease in benthic foraminiferal $\delta^{18}O$, interpreted as 2°C warming of bottom waters. It correlates with increased carbonate dissolution at 2000–3000 m paleodepth in the South Atlantic and Pacific oceans (Figure 7), pointing to a global increase in deep ocean acidity and a rise of the lysocline [*Sexton et al.*, 2011]. A carbonate-barren interval has also been found in the western North Atlantic Ocean (ODP 647, Labrador Sea; Figure 7), extending from just above the highest occurrence of *D. lodoensis* to the C21r/C21n reversal [*Srivastava et al.*, 1989]. *Sexton et al.* [2011] estimated that 650 Gt of carbon derived from methane hydrate dissociation could explain the 0.7–1‰ CIEs of the Ypresian/Lutetian events, but would have been insufficient to cause a deep ocean 2°C warming. They considered that 1600 Gt of carbon released from organic carbon decomposition would be a more plausible explanation. They also observed that these events were generally very short (40 kyr) and had very rapid recovery phases, and concluded that these events represent episodes of dissolved organic carbon oxidation and
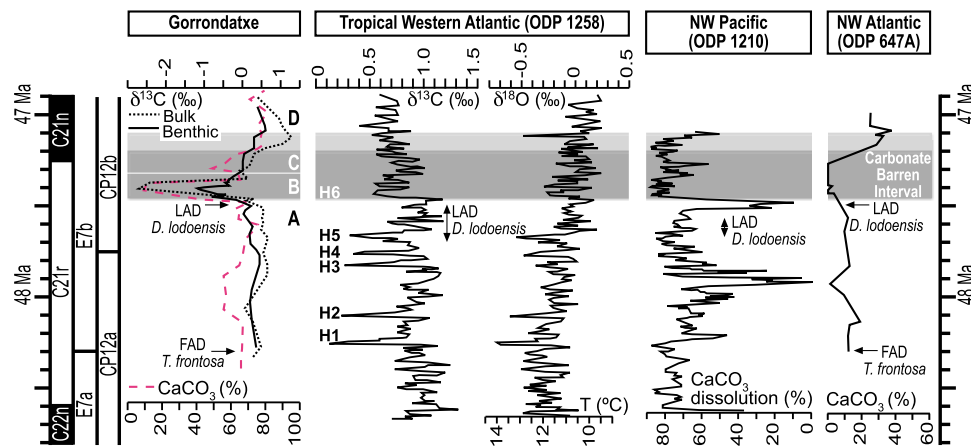
Figure 7. Comparison of the Gorrondatxe geochemical data with those of the tropical western Atlantic record [*Sexton et al.*, 2011], where several events (H1 to H6) were identified within Chron C21r. Correlation is based on magnetostratigraphy, cyclostratigraphy and biostratigraphy (FAD: first appearance datum; LAD: last appearance datum). The onset of the Gorrondatxe environmental perturbation (dark gray box) correlates with the C21r-H6 event, which is marked by a negative CIE in the $\delta^{13}C$ record and involved a deep-sea warming of 2°C according to $\delta^{18}O$ paleotemperatures [*Sexton et al.*, 2011]. The Gorrondatxe perturbation can also be correlated with severe carbonate dissolution episodes in the NW Pacific [*Sexton et al.*, 2011] and in the NW Atlantic [*Srivastava et al.*, 1989]; the return to normal carbonate sedimentation in those oceans was coeval with the aftermath of the C21r-H6 event in Gorrondatxe (light gray box).

redistribution from surficial sediments. However, we noticed that the C21r-H6 event is characterized by a longer-lasting CIE (>100 kyr) and more gradual recovery, as it was followed by a phase of high carbonate dissolution rate that lasted until approximately 47.2 Ma (Chron C21n), thus coinciding in extent with the recovery phase of the Gorrondatxe event (Figure 7).

[38] We conclude that the environmental perturbation recorded at Gorrondatxe was related to the C21r-H6 event defined by *Sexton et al.* [2011]. This was caused by the input of 1600–1700 Gt of ^{13}C-depleted carbon into the ocean-atmosphere system and produced seawater warming and acidification in the Atlantic and Pacific oceans. Our data show that the C21r-H6 event lasted longer than suggested in the original definition, as it extended between 47.44 and 47.214 Ma and included the C21r/C21n transition. This duration is longer than that of most of the other Paleogene carbon-cycle perturbation events (Table 1) and suggests that the isotopically light carbon was derived from external, deeply buried reservoirs [*Norris and Röhl*, 1999; *Zachos et al.*, 2001, 2008; *Dickens*, 2011; *Svensen et al.*, 2004].

[39] The evolutionary patterns and foraminiferal assemblage compositions are similar in the C21r-H6 event at Gorrondatxe and in other Paleogene events [*Stap et al.*, 2010; *Winguth et al.*, 2012], although the PETM remains as the only carbon-cycle perturbation that caused a severe benthic foraminiferal extinction.

[40] The question remains whether the C21r-H6 event was a hyperthermal event, as suggested by *Sexton et al.* [2011]. Benthic foraminiferal $\delta^{18}O$ data reported by these authors and planktic foraminiferal paleobiogeographical indices of Gorrondatxe point to warmer oceans during this event. However, warming above natural variability cannot be demonstrated with the available data (Figure 7). Until a more comprehensive study of this event is undertaken in multiple locations, we can only state that the C21r-H6 event was

caused by a carbon-cycle perturbation similar to those leading to hyperthermal conditions during the early Paleogene.

7. Conclusions

[41] Since the discovery of the PETM event, other similar Paleogene events have been defined. Sedimentological, paleontological and geochemical data from the Gorrondatxe section suggest that a carbon-cycle perturbation (recorded by a −1‰ CIE in the deep-sea benthic foraminiferal $\delta^{13}C$ curve) occurred in early Lutetian times (C21r/C21n transition; from 47.44 to 47.214 Ma of *Gradstein et al.* [2004]). The perturbation caused increased runoff on land, turbidite deposition on the seafloor, and a rise in the lysocline, leading to a proliferation of opportunistic organic-cemented benthic foraminifera; high proportions of low-latitude planktic foraminifera suggest warming of the sea surface. The onset of the Gorrondatxe perturbation correlates with the C21r-H6 event [*Sexton et al.*, 2011], which caused a 2°C warming of the seafloor, and with increased carbonate dissolution in the Atlantic and Pacific oceans. However, the available data is still insufficient to conclude that the environmental perturbation caused global warming outside the parameters of natural variability (i.e., true hyperthermal conditions). Although the duration of the C21r-H6 event suggests that its triggering mechanism may have been similar to that of the PETM, the magnitude of the carbon input and the subsequent environmental perturbation were less severe than during the PETM.

are due to Carl Sheaver for his language corrections. Insightful comments by two anonymous reviewers and Associate Editor R.E. Zeebe helped to improve the original manuscript.

References

Agnini, C., P. Macrì, J. Backman, H. Brinkhuis, E. Fornaciari, L. Giusberti, V. Luciani, D. Rio, A. Sluijs, and F. Speranza (2009), An early Eocene carbon cycle perturbation at ~52.5 Ma in the Southern Alps: Chronology and biotic response, *Paleoceanography*, 24, PA2209, doi:10.1029/2008PA001649.

Alegret, L., and S. Ortiz (2010), El corte de Zumaya (España): Registro de los foraminíferos bentónicos del Paleógeno inferior, *Rev. Mex. Cienc. Geol.*, 27(3), 477–489.

Alegret, L., S. Ortiz, I. Arenillas, and E. Molina (2005), Paleoenvironmental turnover across the Paleocene/Eocene Boundary at the Stratotype section in Dababiya (Egypt) based on benthic foraminifera, *Terra Nova*, 17, 526–536, doi:10.1111/j.1365-3121.2005.00645.x.

Alegret, L., S. Ortiz, X. Orue-Etxebarria, G. Bernaola, J. I. Baceta, S. Monechi, E. Apellaniz, and V. Pujalte (2009a), The Paleocene–Eocene thermal maximum: New data from the microfossil turnover at Zumaia section, *Palaios*, 24, 318–328, doi:10.2110/palo.2008.p08-057r.

Alegret, L., S. Ortiz, and E. Molina (2009b), Extinction and recovery of benthic foraminifera across the Paleocene-Eocene Thermal Maximum at the Alamedilla section (Southern Spain), *Palaeogeogr. Palaeoclimatol. Palaeoecol.*, 279, 186–200, doi:10.1016/j.palaeo.2009.05.009.

Alegret, L., S. Ortiz, I. Arenillas, and E. Molina (2010), What happens when the ocean is overheated? The foraminiferal response across the Paleocene-Eocene Thermal Maximum at the Alamedilla section (Spain), *Geol. Soc. Am. Bull.*, 122, 1616–1624, doi:10.1130/B30055.1.

Bernaola, G., X. Orue-Etxebarria, A. Payros, J. Dinarès-Turell, J. Tosquella, E. Apellaniz, and F. Caballero (2006), Biomagnetostratigraphic analysis of the Gorrondatxe section (Basque Country, western Pyrenees): Its significance for the definition of the Ypresian/Lutetian boundary stratotype, *Neues Jahrb. Geol. Palaeontol. Abh.*, 241, 67–109.

Bernaola, G., J. I. Baceta, X. Orue-Etxebarria, L. Alegret, M. Martín-Rubio, J. Arostegui, and J. Dinarès-Turell (2007), Evidence of an abrupt environmental disruption during the mid-Paleocene biotic event (Zumaia section, western Pyrenees), *Geol. Soc. Am. Bull.*, 119, 785–795, doi:10.1130/B26132.1.

Bijl, P. K., A. J. P. Houben, S. Schouten, S. M. Bohaty, A. Sluijs, G. J. Reichart, J. S. Sinninghe Damsté, and H. Brinkhuis (2010), Transient Middle Eocene atmospheric CO_2 and temperature variations, *Science*, 330, 819–821, doi:10.1126/science.1193654.

Bohaty, S. M., and J. C. Zachos (2003), Significant Southern Ocean warming event in the late middle Eocene, *Geology*, 31, 1017–1020, doi:10.1130/G19800.1.

Bohaty, S. M., J. C. Zachos, F. Florindo, and M. L. Delaney (2009), Coupled greenhouse warming and deep sea acidification in the Middle Eocene, *Paleoceanography*, 24, PA2207, doi:10.1029/2008PA001676.

Bolle, M. P., and T. Adatte (2001), Palaeocene-early Eocene climatic evolution in the Tethyan realm: Clay mineral evidence, *Clay Miner.*, 36, 249–261, doi:10.1180/000985501750177979.

Bornemann, A., P. Schulte, J. Sprong, E. Steurbaut, M. Youssef, and R. P. Speijer (2009), Latest Danian carbon isotope anomaly and associated environmental change in the southern Tethys (Nile basin, Egypt), *J. Geol. Soc.*, 166, 1135–1142, doi:10.1144/0016-76492008-104.

Bowen, G. J., and J. C. Zachos (2010), Rapid carbon sequestration at the termination of the Palaeocene-Eocene Thermal Maximum, *Nat. Geosci.*, 3, 866–869, doi:10.1038/ngeo1014.

Chun, C. O. J., M. L. Delaney, and J. C. Zachos (2010), Paleoredox changes across the Paleocene-Eocene thermal maximum, Walvis Ridge (ODP Sites 1262, 1263, and 1266), Evidence from Mn and U enrichment factors, *Paleoceanography*, 25, PA4202, doi:10.1029/2009PA001861.

Coccioni, R., F. Frontalini, G. Bancalà, E. Fornaciari, L. Jovane, and M. Sprovieri (2010), The Dan-C2 hyperthermal event at Gubio (Italy): Global implications, environmental effects, and cause(s), *Earth Planet. Sci. Lett.*, 297, 298–305, doi:10.1016/j.epsl.2010.06.031.

Colosimo, A. B., T. J. Bralower, and J. C. Zachos (2006), Evidence for lysocline shoaling at the Paleocene/Eocene Thermal Maximum on Shatsky Rise, northwest Pacific, *Proc. Ocean Drill. Program Initial Rep.*, 198, 36 pp., doi:10.2973/odp.proc.sr.198.112.2006.

Cramer, B. S., J. D. Wright, D. V. Kent, and M. P. Aubry (2003), Orbital climate forcing of $\delta^{13}C$ excursions in the late Paleocene-early Eocene (chrons C24n-C25n), *Paleoceanography*, 18(4), 1097, doi:10.1029/2003PA000909.

Dickens, G. R. (2011), Down the rabbit hole: Toward appropriate discussion of methane release from gas hydrate systems during the Paleocene-Eocene thermal maximum and other past hyperthermal events, *Clim. Past*, 7, 831–846, doi:10.5194/cp-7-831-2011.

Dickens, G. R., J. R. O'Neil, D. K. Rea, and R. M. Owen (1995), Dissociation of oceanic methane hydrate as a cause of the carbon isotope excursion at the end of the Paleocene, *Paleoceanography*, 10, 965–971, doi:10.1029/95PA02087.

Dickens, G. R., M. M. Castillo, and C. G. Walker (1997), A blast of gas in the latest Paleocene: Simulating first-order effects of massive dissociation of oceanic methane hydrate, *Geology*, 25, 259–262, doi:10.1130/0091-7613(1997)025<0259:ABOGIT>2.3.CO;2.

Dinarès-Turell, J., J. I. Baceta, G. Bernaola, X. Orue-Etxebarria, and V. Pujalte (2007), Closing the Mid-Paleocene gap: Toward a complete astronomically tuned Paleocene Epoch and Selandian and Thanetian GSSPs at Zumaia (Basque Basin, W Pyrenees), *Earth Planet. Sci. Lett.*, 262, 450–467, doi:10.1016/j.epsl.2007.08.008.

Edgar, K. M., P. A. Wilson, P. F. Sexton, and Y. Suganuma (2007), No extreme bipolar glaciation during the main Eocene calcite compensation shift, *Nature*, 448, 908–911, doi:10.1038/nature06053.

Edgar, K. M., P. A. Wilson, P. F. Sexton, S. J. Gibbs, A. P. Roberts, and R. D. Norris (2010), New biostratigraphic, magnetostratigraphic and isotopic insights into the Middle Eocene Climatic Optimum in low latitudes, *Palaeogeogr. Palaeoclimatol. Palaeoecol.*, 297, 670–682, doi:10.1016/j.palaeo.2010.09.016.

Fontanier, C., F. J. Jorissen, G. Chaillou, P. Anschutz, A. Grémare, and C. Griveaud (2005), Live foraminiferal faunas from a 2800 m deep lower canyon station from the Bay of Biscay: Faunal response to focusing of refractory organic matter, *Deep Sea Res., Part I*, 52, 1189–1227, doi:10.1016/j.dsr.2005.01.006.

Freudenthal, T., T. Wagner, F. Wenzhöfer, M. Zabel, and G. Wefer (2001), Early diagenesis of organic matter from sediments of the eastern subtropical Atlantic: Evidence from stable nitrogen and carbon isotopes, *Geochim. Cosmochim. Acta*, 65, 1795–1808, doi:10.1016/S0016-7037(01)00554-3.

Galeotti, S., S. Krishnan, M. Pagani, L. Lanci, A. Gaudio, J. C. Zachos, S. Monechi, G. Morelli, and L. Lourens (2010), Orbital chronology of Early Eocene hyperthermals from the Contessa Road section, central Italy, *Earth Planet. Sci. Lett.*, 290, 192–200, doi:10.1016/j.epsl.2009.12.021.

Gertsch, B., T. Adatte, G. Keller, A. A. A. M. Tantawy, Z. Berners, H. P. Mort, and D. Fleitmann (2010), Middle and late Cenomanian oceanic anoxic events in shallow and deeper shelf environemnts of western Morocco, *Sedimentology*, 57, 1430–1462, doi:10.1111/j.1365-3091.2010.01151.x.

Giusberti, L., R. Coccioni, M. Sprovieri, and F. Tateo (2009), Perturbation at the sea floor during the Paleocene–Eocene thermal maximum: Evidence from benthic foraminifera at Contessa Road. Italy, *Mar. Micropaleontol.*, 70, 102–119, doi:10.1016/j.marmicro.2008.11.003.

Gradstein, F. M., J. G. Ogg, and A. G. Smith (Eds.) (2004), *A Geologic Time Scale 2004*, Cambridge Univ. Press, Cambridge, U. K., doi:10.4095/215638.

Kauffman, E. G., P. J. Harries, and T. A. Hansen (1996), Models of biotic survival following mass extinction, in *Biotic Recovery from Mass Extinction Events*, edited by M. B. Hart, Geol. Soc. Spec. Publ., 102, 41–60.

Kroeger, K. F., and R. H. Funnell (2012), Warm Eocene climate enhanced petroleum generation from Cretaceous source rocks: A potential climate feedback mechanism? *Geophys. Res. Lett.*, 39, L04701, doi:10.1029/2011GL050345.

Leon-Rodriguez, L., and G. R. Dickens (2010), Constraints on ocean acidification associated with rapid and massive carbon injections: The early Paleogene record at ocean drilling program site 1215, equatorial Pacific Ocean, *Palaeogeogr. Palaeoclimatol. Palaeoecol.*, 298, 409–420, doi:10.1016/j.palaeo.2010.10.029.

Lourens, L. J., A. Sluijs, D. Kroon, J. C. Zachos, E. Thomas, U. Rohl, J. Bowles, and I. Raffi (2005), Astronomical pacing of late Palaeocene to early Eocene global warming events, *Nature*, 435, 1083–1087, doi:10.1038/nature03814.

Luciani, V., L. Giusberti, C. Agnini, E. Formaciari, D. Rio, D. J. A. Spofforth, and H. Pálike (2010), Ecological and evolutionary response of Tethyan planktonic foraminifera to the middle Eocene climatic optimum (MECO) from the Alano section (NE Italy), *Palaeogeogr. Palaeoclimatol. Palaeoecol.*, 292, 82–95, doi:10.1016/j.palaeo.2010.03.029.

Marshall, J. D. (1992), Climatic and oceanographic isotopic signals from the carbonate rock record and their preservation, *Geol. Mag.*, 129, 143–160, doi:10.1017/S0016756800008244.

Molina, E., et al. (2011), The Global Stratotype Section and Point (GSSP) for the base of the Lutetian Stage at the Gorrondatxe section, Spain, *Episodes*, 34, 86–108.

Nguyen, T. M. P., M. R. Petrizzo, P. Stassen, and R. P. Speijer (2011), Dissolution susceptibility of Paleocene-Eocene planktic foraminifera: Implications for palaeoceanographic reconstructions, *Mar. Micropaleontol.*, 81, 1–21, doi:10.1016/j.marmicro.2011.07.001.

Nicolo, M. J., G. R. Dickens, C. J. Hollis, and J. C. Zachos (2007), Multiple early Eocene hyperthermals: Their sedimentary expression on the New Zealand continental margin and in the deep sea, *Geology*, *35*, 699–702, doi:10.1130/G23648A.1.

Norris, R. D., and U. Röhl (1999), Carbon cycling and chronology of climate warming during the Paleocene/Eocene transition, *Nature*, *401*, 775–778, doi:10.1038/44545.

Okada, H., and D. Bukry (1980), Supplementary modification and introduction of code numbers to the low-latitude coccolith biostratigraphic zonation (Bukry, 1973; 1975), *Mar. Micropaleontol.*, *5*, 321–325, doi:10.1016/0377-8398(80)90016-X.

Ortiz, S., L. Alegret, A. Payros, X. Orue-Etxebarria, E. Apellaniz, and E. Molina (2011), Distribution patterns of benthic foraminifera across the Ypresian-Lutetian Gorrondatxe section, Northern Spain: Response to sedimentary disturbance, *Mar. Micropaleontol.*, *78*, 1–13, doi:10.1016/j.marmicro.2010.09.004.

Payros, A., X. Orue-Etxebarria, and V. Pujalte (2006), Covarying sedimentary and biotic fluctuations in Lower-Middle Eocene Pyrenean deep-sea deposits: Palaeoenvironmental implications, *Palaeogeogr. Palaeoclimatol. Palaeoecol.*, *234*, 258–276, doi:10.1016/j.palaeo.2005.10.013.

Payros, A., G. Bernaola, X. Orue-Etxebarria, J. Dinarès-Turell, J. Tosquella, and E. Apellaniz (2007), Reassessment of the Early Middle Eocene biomagnetochronology based on evidence from the Gorrondatxe section (Basque Country, western Pyrenees), *Lethaia*, *40*, 183–195, doi:10.1111/j.1502-3931.2007.00016.x.

Payros, A., X. Orue-Etxebarria, G. Bernaola, E. Apellaniz, J. Dinarès-Turell, J. Tosquella, and F. Caballero (2009a), Characterization and astronomically calibrated age of the first occurrence of *Turborotalia frontosa* in the Gorrondatxe section, a prospective Lutetian GSSP: Implications for the Eocene time scale, *Lethaia*, *42*, 255–264, doi:10.1111/j.1502-3931.2008.00142.x.

Payros, A., J. Tosquella, G. Bernaola, J. Dinarès-Turell, X. Orue-Etxebarria, and V. Pujalte (2009b), Filling the North European Early/Middle Eocene (Ypresian/Lutetian) boundary gap: Insights from the Pyrenean continental to deep-marine record, *Palaeogeogr. Palaeoclimatol. Palaeoecol.*, *280*, 313–332, doi:10.1016/j.palaeo.2009.06.018.

Payros, A., J. Dinarès-Turell, G. Bernaola, X. Orue-Etxebarria, E. Apellaniz, and J. Tosquella (2011), On the age of the Early/Middle Eocene boundary and other related events: Cyclostratigraphic refinements from the Pyrenean Otsakar section and the Lutetian GSSP, *Geol. Mag.*, *148*, 442–460, doi:10.1017/S0016756810000890.

Petrizzo, M. R. (2005), An early late Paleocene event on Shatsky Rise, northwest Pacific Ocean (ODP Leg 198), Evidence from planktonic foraminiferal assemblages, *Proc. Ocean Drill. Program Sci. Results*, *198*, 29 pp., doi:10.2973/odp.proc.sr.198.102.2005.

Quillévéré, F., R. D. Norris, D. Kroon, and P. A. Wilson (2008), Transient ocean warming and shifts in carbon reservoirs during the early Danian, *Earth Planet. Sci. Lett.*, *265*, 600–615, doi:10.1016/j.epsl.2007.10.040.

Reuning, L., J. J. G. Reijmer, and C. Betzler (2002), Sedimentation cycles and their diagenesis on the slope of a Miocene carbonate ramp (Bahamas, ODP Leg 166), *Mar. Geol.*, *185*, 121–142, doi:10.1016/S0025-3227(01)00293-6.

Reuning, L., J. J. G. Reijmer, C. Betzler, P. Swart, and T. Bauch (2005), The use of paleoceanographic proxies in carbonate periplatform settings–opportunities and pitfalls, *Sediment. Geol.*, *175*, 131–152, doi:10.1016/j.sedgeo.2004.12.026.

Ridgwell, A., and U. Edwards (2007), Geological carbon sinks, in *Greenhouse Gas Sinks*, edited by D. Reay et al., pp. 74–97, CABI, Wallingford, U. K., doi:10.1079/9781845931896.0074.

Ridgwell, A., and D. N. Schmidt (2010), Past constraints on the vulnerability of marine calcifiers to massive carbon dioxide release, *Nat. Geosci.*, *3*, 196–200, doi:10.1038/ngeo755.

Robert, C., and J. P. Kennett (1992), Paleocene and Eocene kaolinite distribution in the South Atlantic and Southern Ocean: Antarctic climatic and paleoceanographic implications, *Mar. Geol.*, *103*, 99–110, doi:10.1016/0025-3227(92)90010-F.

Robert, C., and J. P. Kennett (1994), Antarctic subtropical humid episode at the Paleocene-Eocene boundary: Clay mineral evidence, *Geology*, *22*, 211–214, doi:10.1130/0091-7613(1994)022<0211:ASHEAT>2.3.CO;2.

Rodríguez-Tovar, F. J., A. Uchman, A. Payros, X. Orue-Etxebarria, E. Apellaniz, and E. Molina (2010), Sea-level dynamics and palaeoecological factors affecting trace fossil distribution in Eocene turbiditic deposits from the Gorrondatxe section, N Spain, *Palaeogeogr. Palaeoclimatol., Palaeoecol.*, *285*, 50–65, doi:10.1016/j.palaeo.2009.10.022.

Röhl, U., T. Westerhold, T. J. Bralower, and J. C. Zachos (2007), On the duration of the Paleocene-Eocene thermal maximum (PETM), *Geochem. Geophys. Geosyst.*, *8*, Q12002, doi:10.1029/2007GC001784.

Schmitz, B., and V. Pujalte (2003), Sea-level, humidity, and land-erosion records across the initial Eocene thermal maximum from a continental-marine transect in northern Spain, *Geology*, *31*, 689–692, doi:10.1130/G19527.1.

Schmitz, B., and V. Pujalte (2007), Abrupt increase in seasonal extreme precipitation at the Paleocene-Eocene boundary, *Geology*, *35*, 215–218, doi:10.1130/G23261A.1.

Schmitz, B., F. Asaro, E. Molina, S. Monechi, K. von Salis, and R. P. Speijer (1997), High-resolution iridium, $\delta^{13}C$, $\delta^{18}O$, foraminifera and nannofossil profiles across the latest Paleocene benthic extinction event at Zumaya, Spain, *Palaeogeogr. Palaeoclimatol. Palaeoecol.*, *133*, 49–68, doi:10.1016/S0031-0182(97)00024-2.

Schmitz, B., V. Pujalte, and K. Nuñez-Betelu (2001), Climate and sea-level perturbations during the Initial Eocene Thermal Maximum: Evidence from siliciclastic units in the Basque Basin (Ermua and Trabakua Pass), northern Spain, *Palaeogeogr. Palaeoclimatol. Palaeoecol.*, *165*, 299–320, doi:10.1016/S0031-0182(00)00167-X.

Sexton, P. F., R. D. Norris, P. A. Wilson, H. Pälike, T. Westerhold, U. Röhl, C. T. Bolton, and S. Gibbs (2011), Eocene global warming events driven by ventilation of oceanic dissolved organic carbon, *Nature*, *471*, 349–352, doi:10.1038/nature09826.

Sluijs, A., S. Schouten, T. H. Donders, P. L. Schoon, U. Röhl, G. J. Reichart, F. Sangiorgi, J. H. Kim, J. S. Sinninghe Damsté, and H. Brinkhuis (2009), Warm and wet conditions in the Arctic region during Eocene Thermal Maximum 2, *Nat. Geosci.*, *2*, 777–780, doi:10.1038/ngeo668.

Sluijs, A., P. K. Bijl, S. Schouten, U. Röhl, G. J. Reichart, and H. Brinkhuis (2011), Southern ocean warming, sea level and hydrological change during the Paleocene-Eocene thermal maximum, *Clim. Past.*, *7*, 47–61, doi:10.5194/cp-7-47-2011.

Spofforth, D. J. A., C. Agnini, H. Pälike, D. Rio, E. Fornaciari, L. Giusberti, V. Luciani, L. Lanci, and G. Muttoni (2010), Organic carbon burial following the middle Eocene climatic optimum in the central western Tethys, *Paleoceanography*, *25*, PA3210, doi:10.1029/2009PA001738.

Sprong, J., M. A. Youssef, A. Bornemann, P. Schulte, E. Steurbaut, P. Stassen, T. J. Kouwenhoven, and R. P. Speijer (2011), A multi-proxy record of the Latest Danian Event at Gebel Qreiya, Eastern Desert, Egypt, *J. Micropaleontol.*, *30*, 167–182, doi:10.1144/0262-821X10-023.

Sprong, J., T. J. Kouwenhoven, A. Bornemann, P. Schulte, P. Stassen, E. Steurbaut, M. Youssef, and R. P. Speijer (2012), Characterization of the Latest Danian Event by means of benthic foraminiferal assemblages along a depth transect at the southern tethyan margin (Nile Basin, Egypt), *Mar. Micropaleontol.*, *86–87*, 15–31, doi:10.1016/j.marmicro.2012.01.001.

Srivastava, S. P., et al. (1989), *Proceedings of the Ocean Drilling Program, Scientific Results*, vol. 105, Ocean Drill. Program, College Station, Tex., doi:10.2973/odp.proc.sr.105.1989.

Stap, L., A. Sluijs, E. Thomas, and L. Lourens (2009), Patterns and magnitude of deep sea carbonate dissolution during Eocene Thermal Maximum 2 and H2, Walvis Ridge, South-Eastern Atlantic Ocean, *Paleoceanography*, *24*, PA1211, doi:10.1029/2008PA001655.

Stap, L., L. J. Lourens, E. Thomas, A. Sluijs, S. Bohaty, and J. C. Zachos (2010), High-resolution deep-sea carbon and oxygen isotope records of Eocene Thermal Maximum 2 and H2, *Geology*, *38*, 607–610, doi:10.1130/G30777.1.

Svensen, H., S. Planke, A. Malthe-Sorenssen, B. Jamtveit, R. Myklebust, T. Rasmussen Eldem, and S. S. Rey (2004), Release of methane from a volcanic basin as a mechanism for the initial Eocene global warming, *Nature*, *429*, 542–545, doi:10.1038/nature02566.

Thiry, M. (2000), Palaeoclimatic interpretation of clay minierals in marine deposits: An outlook from the continental origin, *Earth Sci. Rev.*, *49*, 201–221, doi:10.1016/S0012-8252(99)00054-9.

Thomas, E. (2003), Extinction and food at the sea floor: A high-resolution benthic foraminiferal record across the Initial Eocene Thermal Maximum, Southern Ocean Site 690, in *Causes and Consequences of Globally Warm Climates of the Paleogene*, edited by S. Wing et al., *Spec. Pap. Geol. Soc. Am.*, *369*, 319–332, doi:10.1130/0-8137-2369-8.319.

Thomas, E. (2007), Cenozoic mass extinctions in the deep sea; what disturbs the largest habitat on Earth?, in *Large Ecosystem Perturbations: Causes and Consequences*, edited by S. Monechi, R. Coccioni, and M. Rampino, *Spec. Pap. Geol. Soc. Am.*, *424*, 1–23, doi:10.1130/2007.2424(01).

Wade, B. S., P. N. Pearson, W. A. Berggren, and H. Pälike (2011), Review and revision of Cenozoic tropical planktonic foraminiferal biostratigraphy and calibration to the geomagnetic polarity and astronomical time scale, *Earth Sci. Rev.*, *104*, 111–142, doi:10.1016/j.earscirev.2010.09.003.

Westerhold, T., U. Röhl, B. Donner, H. K. McCarren, and J. C. Zachos (2011), A complete high-resolution Paleocene benthic stable isotope record for the central Pacific (ODP Site 1209), *Paleoceanography*, *26*, PA2216, doi:10.1029/2010PA002092.

Winguth, A. M. E., E. Thomas, and C. Winguth (2012), Global decline in ocean ventilation, oxygenation, and productivity during the Paleocene-

Eocene Thermal Maximum: Implications for the benthic extinction, *Geology*, *40*, 263–266, doi:10.1130/G32529.1.

Zachos, J., M. Pagani, L. Sloan, E. Thomas, and K. Billups (2001), Trends, rhythms, and aberrations in global climate 65 Ma to Present, *Science*, *292*, 686–693, doi:10.1126/science.1059412.

Zachos, J. C., et al. (2005), Rapid acidification of the ocean during the Paleocene-Eocene Thermal Maximum, *Science*, *308*, 1611–1615, doi:10.1126/science.1109004.

Zachos, J. C., G. R. Dickens, and R. E. Zeebe (2008), An early Cenozoic perspective on greenhouse warming and carbon-cycle dynamics, *Nature*, *451*, 279–283, doi:10.1038/nature06588.

Zachos, J. C., H. McCarren, B. Murphy, U. Röhl, and T. Westerhold (2010), Tempo and scale of late Paleocene and early Eocene carbon isotope cycles: Implications for the origin of hyperthermals, *Earth Planet. Sci. Lett.*, *299*, 242–249, doi:10.1016/j.epsl.2010.09.004.

Zeebe, R. E. (2012), LOSCAR: Long-term ocean-atmosphere-sediment carbon cycle reservoir model v2.0.4, *Geosci. Model Dev.*, *5*, 149–166, doi:10.5194/gmd-5-149-2012.